A Linear Quadratic Regulator with Optimal Reference Tracking for Three-Phase Inverter-Based Islanded Microgrids

Patarroyo-Montenegro, Juan F.; Andrade, Fabio; Guerrero, Josep M.; Vasquez, Juan C.

Published in:
IEEE Transactions on Power Electronics

DOI (link to publication from Publisher):
10.1109/TPEL.2020.3036594

Publication date:
2021

Document Version
Publisher's PDF, also known as Version of record

A Linear Quadratic Regulator With Optimal Reference Tracking for Three-Phase Inverter-Based Islanded Microgrids

Juan F. Patarroyo-Montenegro, *Member, IEEE*, Fabio Andrade, *Member, IEEE*, Josep M. Guerrero, *Fellow, IEEE*, and Juan C. Vasquez, *Senior Member, IEEE*

***Abstract*—This article proposes a power sharing control method based on the linear quadratic regulator with optimal reference tracking (LQR-ORT) for three-phase inverter-based generators using inductor-capacitor-inductor (LCL) filters islanded mode. Compared to single-input single-output (SISO)-based controllers, the LQR-ORT controller increases robustness margins and reduces the quadratic value of the power error and control inputs during transient response. Supplementary loops are used to reduce frequency and voltage deviations in the ac bus without communications. The supplementary loop for voltage regulation is based on the droop controller by reducing direct and quadrature output voltages according to the active and reactive power demand. A model in a synchronous reference frame that integrates power sharing and voltage–current dynamics is also proposed. In addition, a methodology to develop an islanded microgrid model in a synchronous reference frame is proposed. Robustness analysis demonstrates stability of the LQR-ORT controller under variations in the frequency and the LCL filter components. Experimental results demonstrate accuracy of the proposed model and the effectiveness of the LQR-ORT controller on improving transient response and robustness in islanded mode.**

***Index Terms*—Grid-connected mode, inverter-based generators, islanded mode, linear quadratic regulator (LQR), microgrids, modeling, optimal control, power sharing, voltage regulation.**

I. Introduction

THE droop controller has been the most popular control method for regulating active and reactive power sharing in parallel connected voltage-source inverters (VSI) for microgrid applications. In the last decade, this method has been preferred because it allows the distribution of power generation among VSIs proportionally without communications [1]–[7]. Typically, droop controllers reduce frequency and voltage amplitude in order to share active and reactive power, similarly to synchronous generators. Though this method only uses local variables, there are a number of stability issues that have been addressed through time [4], [5], [8], [9].

One of the most important issues related to droop control is the need of a low-pass filter (LPF) to separate the dynamics of the primary control level from the voltage–current ($V-I$) control level [10]. The LPF is also used to calculate the mean value of the instantaneous active and reactive power. The relatively small bandwidth of the LPF inserts a pair of eigenvalues located close to the imaginary axis, which makes the VSI prone to instability if the droop gains and the cutoff frequency are not appropriately selected as demonstrated in [11]–[14].

The use of the LPF also affects the transient response of the voltage and frequency in the ac bus under load changes. To overcome this, a current sharing method using virtual impedance in a synchronous reference frame has been proposed [8], [15], [16]. This method allows to obtain faster responses and improved current decoupling compared to the conventional droop controller. However, the active and reactive powers are not directly controlled, which may cause inaccuracies when sharing loads between VSIs.

Another important issue regarding conventional droop control is that the droop gains and $V-I$ control parameters are typically found using heuristic methods. Some approaches developed closed-loop small-signal models to determine the location of the eigenvalues associated to droop dynamics, neglecting inner loop eigenvalues, and power coupling [4], [13], [17]–[21]. This neglect results in model inaccuracies when describing VSI robustness and performance. Also, the closed-loop models for droop control do not allow the implementation of some important robustness and stability estimation methods, such as singular value diagrams or gain-phase margin estimation.

Most of the closed-loop models used to design droop controllers do not allow to design model-based controller methods such as linear quadratic (LQ) control, H_∞-based control, or model predictive control (MPC). These methods are aimed to improve closed-loop stability, performance, and robustness [22], [23]. Some important contributions related to optimal control

Manuscript received June 14, 2020; revised August 29, 2020; accepted October 22, 2020. Date of publication November 6, 2020; date of current version February 5, 2021. This work was supported in part by the U.S. Department of Energy under Grant DE-SC0020281 and in part by the VILLUM FONDEN under the VILLUM Investigator Grant 25920: Center for Research on Microgrids (CROM). Recommended for publication by Associate Editor G. Escobar. *(Corresponding author: Juan F. Patarroyo-Montenegro.)*

Juan F. Patarroyo-Montenegro and Fabio Andrade are with the Electrical and Computer Engineering Department, University of Puerto Rico at Mayaguez, Mayaguez, PR 00680 USA (e-mail: juan.patarroyo@upr.edu; fabio.andrade@upr.edu).

Josep M. Guerrero and Juan C. Vasquez are with the Department of Energy Technology, Center for Research on Microgrids (CROM), Aalborg University, 9220 Aalborg East, Denmark (e-mail: joz@et.aau.dk; juq@et.aau.dk).

Color versions of one or more of the figures in this article are available online at https://ieeexplore.ieee.org.

Digital Object Identifier 10.1109/TPEL.2020.3036594

methods for VSI power sharing control have been developed [24]–[29]. Most of these approaches rely on the use of an LPF inside the control loop to regulate active and reactive power. In [27], the closed-loop eigenvalue location of the droop controller is maximized using a flatness-based controller. Although this controller enhances voltage total harmonic distortion THD and stability, it requires a global positioning system to synchronize VSIs. In [28], a fuzzy controller with a particle swarm optimization algorithm is proposed to improve reactive power sharing. However, although this method improves reactive power transient response, it relies on the use of an LPF to calculate active and reactive power. Also, the fuzzy-based controllers do not allow the stability or robustness analysis to be performed on the closed-loop system. In [29], a droop-free controller using a nonlinear optimization method is used to achieve optimal power dispatch, adequate power sharing, and minimization of the voltage in the ac bus. In addition, the authors propose a novel model for optimizing their control objectives. However, the whole controller relies on a centralized microgrid controller and a cooperative communication link, which reduces reliability.

To cope with the aforementioned, this article presents an optimal LQ control method with optimal reference tracking (LQR-ORT) that integrates $V{-}I$ and primary control levels for three-phase inverter-based microgrids. This controller is able to operate in grid-connected and islanded mode. Performance of the proposed LQR-ORT controller in grid-connected mode is presented in [30]. Supplementary loops are used to regulate frequency and voltage amplitude in islanded mode. The supplementary loop that regulates voltage amplitude is also used to regulate power sharing among inverters. This supplementary loop is based on the droop control concept by drooping direct and quadrature output voltages according to active and reactive power, respectively. To compute the LQR-ORT controller of each generator, a model in a synchronous *dq* frame that combines power sharing and $V{-}I$ dynamics is presented. Also, robustness of the entire microgrid is assessed by using robustness analysis techniques such as robustness margins estimations under frequency and load and variations. Other applications regarding stability and robustness analysis of this model are presented in [31].

Compared to similar approaches found in literature, this article has the following advantages. First, this approach is intended to minimize the energy in the states and inputs for the $V{-}I$ and primary control level using a single controller, which means better transient response, reduced tracking error, and less power losses during transient responses. Second, the use of an LQR controller has many robustness benefits regarding the gain and phase margins [22]. Third, the supplementary loop to regulate microgrid frequency allows each inverter to operate in islanded mode in a synchronous frame without affecting frequency stability. Fourth, the proposed state-space model allows the performance of stability and robustness analysis to each generator and the entire microgrid in a comprehensive way. Finally, in contrast to conventional droop controllers, the proposed controller does not use resonant filters for the $V{-}I$ level or LPFs for power estimation in the primary level. Thus, the robustness and stability of the microgrid is improved.

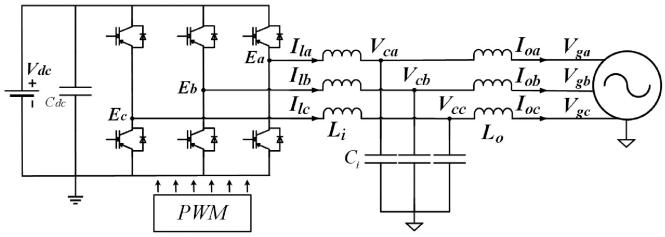

Fig. 1. Three-phase generator connected to a voltage source.

Furthermore, transient responses of the frequency and the voltage amplitude in the ac bus are improved.

The rest of this article is organized as follows. Section II presents the mathematical models used to develop the proposed controller. In Section III, the proposed controller and the supplementary loops for regulating frequency and voltage in the ac bus are presented. Section IV presents robustness and stability analysis for a proposed experimental microgrid. Also, a test case in a real test bench is shown in this section. Finally, the conclusion is presented in Section V.

II. Mathematical Model

The model of each inverter connected to the main grid is used to describe dynamics in grid-connected mode. This model is also used to develop the proposed control strategy. Then, the models of all inverters are integrated in a single state-space model to describe microgrid dynamics in islanded mode.

A. Model of a Single Inverter Connected to the Main Grid

The circuit used to develop the proposed model in grid-connected mode is shown in Fig. 1. The output of the three-phase inverter E_{abc} is connected using an inductor-capacitor-inductor (LCL) output filter to a voltage source V_{gabc} that represents the ac bus. Input inductor current, capacitor voltage, and output current are denoted by I_{labc}, V_{cabc}, and I_{oabc} respectively. The differential equations for one phase of this circuit are given by

$$C\,\frac{dV_c}{dt} = I_l - I_o;\;\; L_i\,\frac{dI_l}{dt} = E - V_c;\;\; L_o\,\frac{dI_o}{dt} = V_c - V_g \tag{1}$$

with L_i, L_o, and C being the input inductance, output inductance, and capacitor, respectively. The state-space model of this circuit for each phase in the *ABC* frame is given by

$$\begin{bmatrix}\dot{V}_c\\ \dot{I}_l\\ \dot{I}_o\end{bmatrix} = \begin{bmatrix}0 & 1/C & -1/C\\ -1/L_i & 0 & 0\\ 1/L_o & 0 & 0\end{bmatrix}\begin{bmatrix}V_c\\ I_l\\ I_o\end{bmatrix} + \begin{bmatrix}0\\ 1/Li\\ 0\end{bmatrix}E + \begin{bmatrix}0\\ 0\\ -1/L_o\end{bmatrix}V_g. \tag{2}$$

The state-space model (3) is obtained using the *dq* transformation at the nominal angular frequency ω_c (see Appendix).

$$\overbrace{\begin{bmatrix}\dot{V}_{cd}\\ \dot{V}_{cq}\\ \dot{I}_{ld}\\ \dot{I}_{lq}\\ \dot{I}_{od}\\ \dot{I}_{oq}\end{bmatrix}}^{\dot{x}_{dq}} = \overbrace{\begin{bmatrix} 0 & \omega_c & 1/C & 0 & -1/C & 0\\ -\omega_c & 0 & 0 & 1/C & 0 & -1/C\\ -1/L_i & 0 & 0 & \omega_c & 0 & 0\\ 0 & -1/L_i & -\omega_c & 0 & 0 & 0\\ 1/L_o & 0 & 0 & 0 & 0 & \omega_c\\ 0 & 1/L_o & 0 & 0 & -\omega_c & 0\end{bmatrix}}^{A_{dq}} \overbrace{\begin{bmatrix}V_{cd}\\ V_{cq}\\ I_{ld}\\ I_{lq}\\ I_{od}\\ I_{oq}\end{bmatrix}}^{x_{dq}} + \overbrace{\begin{bmatrix} 0 & 0\\ 0 & 0\\ 1/L_i & 0\\ 0 & 1/L_i\\ 0 & 0\\ 0 & 0\end{bmatrix}}^{B_{1dq}} \overbrace{\begin{bmatrix}E_d\\ E_q\end{bmatrix}}^{E_{dq}} + \overbrace{\begin{bmatrix} 0 & 0\\ 0 & 0\\ 0 & 0\\ 0 & 0\\ -1/L_o & 0\\ 0 & -1/L_o\end{bmatrix}}^{B_{2dq}} \overbrace{\begin{bmatrix}V_{gd}\\ V_{gq}\end{bmatrix}}^{V_{gdq}}. \tag{3}$$

The active power P and reactive power Q are defined by [32]

$$P = 1.5\left(V_{gd}I_d + V_{gq}I_q\right) \tag{4}$$

$$Q = 1.5\left(V_{gq}I_d - V_{gd}I_q\right). \tag{5}$$

According to grid regulations such as IEEE 1547 [33], it is correct to assume that V_{gdq} will have small deviations around the operating point $V_{gdq} = [\,\bar{V}_{gd}\;0\,]$, where $\bar{V}_{gd}$ represents the nominal peak amplitude of the ac bus. The *dq* frame is synchronized with the phase A of the ac bus (V_{ga}) using a phase-locked loop (PLL) so that $V_{gq} = 0$ [32]. Thus, the active and reactive power can be written as a linearized equation as follows:

$$y = \begin{bmatrix}P\\ Q\end{bmatrix} = 1.5\begin{bmatrix}\bar{V}_{gd} & 0\\ 0 & -\bar{V}_{gd}\end{bmatrix}\begin{bmatrix}I_{od}\\ I_{oq}\end{bmatrix}. \tag{6}$$

To discretize the state-space model, the delay induced by the pulsewidth modulation (PWM) switching must be considered [34]. This is done by using a delay block or a discrete-time backward integrator. The discrete-time backward integrator also allows the reduction of the steady-state error in the closed-loop system. The augmented system using a backward integrator in the input is given by

$$X\;[k{+}1] = \begin{bmatrix}\bar{A}_{dq} & \bar{B}_{1dq}\\ 0_{2\times 6} & I_{2\times 2}\end{bmatrix} X\,[k] + \begin{bmatrix}0_{6\times 2}\\ T_s I_{2\times 2}\end{bmatrix} E_{dq}\,[k] + \bar{B}_{2dq}V_{gdq}\,[k] \tag{7}$$

where $X = [\,x_{dq}\;E_{idq}\,]^{\mathrm{T}}$, the auxiliary integral of the input is represented by E_{idq}, T_s is the sampling period, and the upper bar ■ represents the discrete-time transformation [22]. Thus, the discrete-time state-space system can be rewritten as

$$X\;[k+1] = \bar{A}_T\,X\,[k] + \bar{B}_{1T}E_{dq}\,[k] + \bar{B}_{2dq}V_{gdq}\,[k]$$
$$y = CX\,[k]. \tag{8}$$

According to (6), the output matrix C is given by

$$C = 1.5\begin{bmatrix}0 & 0 & 0 & 0 & \bar{V}_{gd} & 0 & 0 & 0\\ 0 & 0 & 0 & 0 & 0 & -\bar{V}_{gd} & 0 & 0\end{bmatrix}. \tag{9}$$

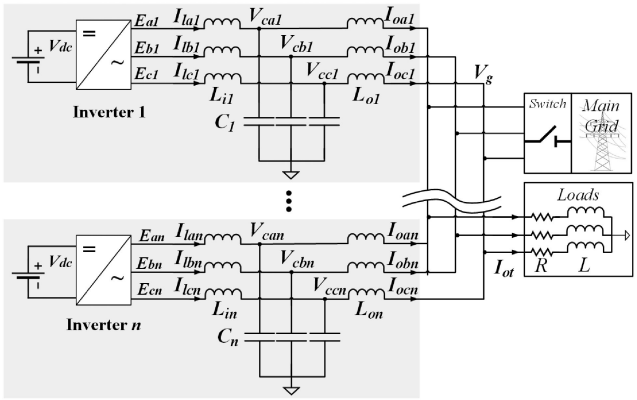

Fig. 2. Control scheme for the LQR-ORT controller.

B. Model of the Microgrid in Islanded Mode

The complete microgrid model is used to assess stability and robustness in islanded mode. Other applications regarding stability and robustness analysis of this model have been presented in [31]. The circuit considered for the islanded microgrid model is shown in Fig. 2. The load was selected to be a series RL circuit in order to analyze dynamics of the active and reactive power. To obtain the complete microgrid model, the model of each inverter must be computed separately by using (2). Then, V_g must be defined in terms of the output currents and load components as follows:

$$V_g = L\dot{I}_{ot} + RI_{ot} \tag{10}$$

where $I_{ot} = \sum_{j=1}^{n} I_{oj}$, for n generators. From (1), the output current dynamics for each generator are given by

$$L_o\,\dot{I}_o = V_c - V_g\,. \tag{11}$$

Evaluating V_g from (10) into (11) for each generator yields to (12). For the *j*th generator, φ_j represents a row vector of size *n* with the coefficients of each state variable properly arranged from the solution of (12)

$$\begin{bmatrix}\dot{I}_{o1}\\ \vdots\\ \dot{I}_{on}\end{bmatrix} = \begin{bmatrix}(L_{o1}+L) & L & L\\ L & \ddots & L\\ L & L & (L_{on}+L)\end{bmatrix}^{-1}\begin{bmatrix}V_{c1}-RI_{ot}\\ \vdots\\ V_{cn}-RI_{ot}\end{bmatrix} = \begin{bmatrix}\varphi_1\\ \vdots\\ \varphi_n\end{bmatrix}\begin{bmatrix}V_{c1}\\ I_{l1}\\ I_{o1}\\ \vdots\\ V_{cn}\\ I_{ln}\\ I_{on}\end{bmatrix}. \tag{12}$$

Combining the solution of (12) with the model of each generator (2), the complete microgrid model (13) is obtained as

follows:

$$\begin{bmatrix} \dot{V}_{c1} \\ \dot{I}_{l1} \\ \dot{I}_{o1} \\ \vdots \\ \dot{V}_{cn} \\ \dot{I}_{ln} \\ \dot{I}_{on} \end{bmatrix} = \begin{bmatrix} \tilde{A}_1 & 0_{2\times3} & \dots & \dots & 0_{2\times3} \\ & & \varphi_1 & & \\ 0_{2\times3} & \dots & \tilde{A}_2 & \dots & 0_{2\times3} \\ & & \varphi_2 & & \\ \vdots & \vdots & \vdots & \vdots & \vdots \\ 0_{2\times3} & \dots & \dots & 0_{2\times3} & \tilde{A}_n \\ & & \varphi_n & & \end{bmatrix} \begin{bmatrix} V_{c1} \\ I_{l1} \\ I_{o1} \\ \vdots \\ V_{cn} \\ I_{ln} \\ I_{on} \end{bmatrix} + \begin{bmatrix} B_1 & \dots & 0_{3\times1} \\ \vdots & \ddots & \vdots \\ 0_{3\times1} & \dots & B_n \end{bmatrix} \begin{bmatrix} E_1 \\ \vdots \\ E_n \end{bmatrix} \tag{13}$$

where

$$\tilde{A}_j = \begin{bmatrix} 0 & 1/C_j & -1/C_j \\ -1/L_{ij} & 0 & 0 \end{bmatrix}, \; B_j = \begin{bmatrix} 0 \\ \frac{1}{L_{ij}} \\ 0 \end{bmatrix}, \forall 1 \leq j \leq n. \tag{14}$$

The model (13) is for each phase. However, it must be transformed to the *dq* frame using (35) from the Appendix.

III. Integrated Optimal Controller

The complete scheme for the integrated optimal controller is shown in Fig. 3. The LQR-ORT feedback matrix K_d and the optimal tracking matrix $K_\nu\nu$ are used to regulate the output power of each generator. If the grid is suddenly disconnected, the grid connection flag is set to zero and the voltage controller and the droop controller are activated. These controllers are used to regulate voltage and load sharing among generators in islanded mode. In addition, the grid connection flag sets the PLL to islanded mode in order to regulate frequency deviations.

A. Computation of the LQR Controller

The discrete-time LQR-ORT optimization problem defines a cost function that weighs the sum of squares of the system input $E_{dq}[k]$ and the output error $e\,[k] = Y[k] - r[k]$. The discrete LQR-ORT cost function is given by [22]

$$J\,(k_o) = \frac{1}{2} \sum_{k=k_0}^{T} \left(e[k]^T Q_p e\,[k] + E_{dq}^T\,[k]\, R_p E_{dq}\,[k] \right). \tag{15}$$

The matrix Q_p is symmetric positive semidefinite and R_p is a symmetric positive definite matrix. Notice that unlike classic LQR approaches, the cost function (15) only includes input and error signals and does not include the state vector $X[k]$. To solve this minimization problem, the modified discrete algebraic Ricatti equation must be solved [22]

$$S = \bar{A}_T^T\, S\left(\bar{A}_T - \bar{B}_{1T} K_d\right) + C^T Q_p C. \tag{16}$$

The optimal state-feedback controller matrix is given by

$$K_d = \left(\bar{B}_{1T}^T S \bar{B}_{1T} + R_p\right)^{-1} \bar{B}_{1T}^T S \bar{A}_T. \tag{17}$$

B. Optimal Reference Tracking Matrix

The reference signal $r[k]$ introduces an additional difference equation to the optimization problem to minimize tracking error.

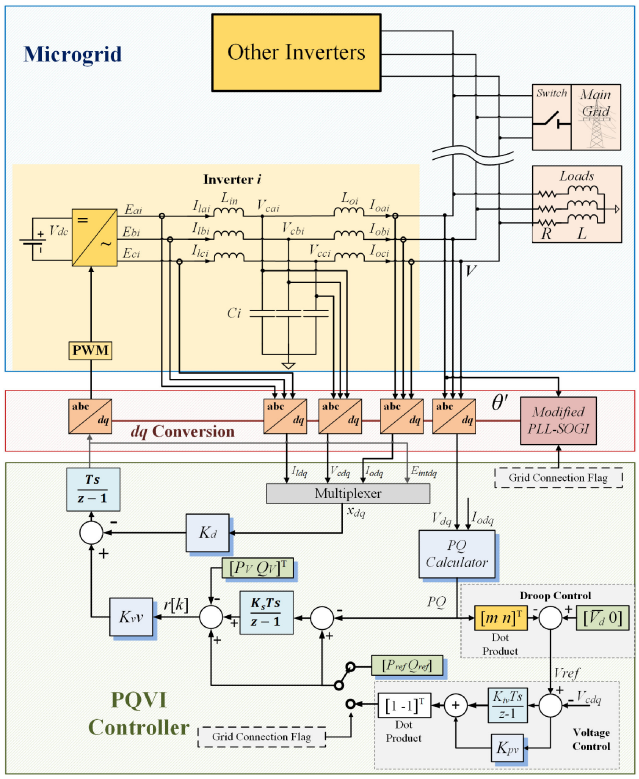

Fig. 3. Complete islanded microgrid scheme with an *RL* load.

This equation is solved offline to obtain a control law that minimizes (15) [22]

$$\nu\;[k+1] = \left(\bar{A}_T - \bar{B}_{1T} K_d\right)^{\mathrm{T}} \nu\,[k] + C^{\mathrm{T}} Q_p r\,[k] \tag{18}$$

where ν is an auxiliary matrix similar to S. A static value of ν is obtained assuming a step reference signal $r[k]$, and solving (18) with infinite horizon such that $\nu\,[k] = \nu[k+1]$

$$\nu = \left[I - \left(\bar{A}_T - \bar{B}_{1T} K_d\right)^{\mathrm{T}}\right]^{-1} C^{\mathrm{T}} Q_p. \tag{19}$$

The control law for the LQR-ORT problem is defined by

$$E_{dq}\,[k] = \left(\bar{B}_{1T}^{\mathrm{T}} S \bar{B}_{1T} + R_p\right)^{-1} \bar{B}_{1T}^{\mathrm{T}} \left(-S \bar{A}_T X\,[k] + \nu r\,[k]\right). \tag{20}$$

Defining $K_v = (\bar{B}_{1T}^{\mathrm{T}} S \bar{B}_{1T} + R_p)^{-1}\, \bar{B}_{1T}^{\mathrm{T}}$ and replacing K_d from (17) into (20) results in a compact form of the control law as shown in the following:

$$E_{dq} = -K_d X\,[k] + K_v \nu r\,[k]. \tag{21}$$

The product $K_\nu\nu$ is known as the ORT. As shown in Fig. 3, this matrix transforms a vector in the units of $r[k]$ to a vector in the units of $E_{dq}[k]$ such that (15) is minimized.

C. Main Grid Power Contribution Calculation Using Superposition Principle

As V_{gdq} is not considered in (15) to compute the LQR-ORT controller, its effects on the injected power must be subtracted from the raw reference signal $[\,P_{\mathrm{ref}}\;Q_{\mathrm{ref}}\,]^{\mathrm{T}}$ to obtain the net power reference $r[k]$ as shown in Fig. 3. Thus, the superposition

principle must be applied to the closed-loop system as follows:

$$X\ [k{+}1] = (\bar{A}_T\ - \bar{B}_T K_d)\, X\,[k] + \bar{B}_{1T} K_\nu \nu r\,[k] + \bar{B}_{2dq} V_{gdq}. \tag{22}$$

To analyze the power contribution of V_{gdq}, the closed-loop system (22) must be simulated with $r\,[k] = [0 \quad 0]^{\mathrm{T}}$. The power contribution of V_{gdq} is computed using the expression

$$Y_V = \begin{bmatrix} P_V \\ Q_V \end{bmatrix} = \begin{bmatrix} \bar{V}_{gd} & 0 \\ 0 & -\bar{V}_{gd} \end{bmatrix} \begin{bmatrix} \bar{\bar{I}}_{od} \\ \bar{\bar{I}}_{oq} \end{bmatrix} \tag{23}$$

where $\bar{\bar{I}}_{od}$ and $\bar{\bar{I}}_{oq}$ are the output current values when (22) reaches steady state with nominal values of V_{gdq}.

Since Y_V and $K_\nu \nu$ are computed offline based on ideal components, there may be slight deviations in the experimental steady-state output values. One way to address this issue is to represent the external input as a stochastic current signal [35]. However, as the LQR-ORT is intended to work in islanded mode, the external input should be expressed as a voltage input. To avoid deviations in the output power caused by disturbances in the ac bus, the integral of the power error is added to $r[k]$ as shown in Fig. 3. This integral is calculated using a low gain K_s to not affect stability margins nor transient response.

The net reference $R[z]$ is then defined as follows:

$$R\,(z) = \begin{bmatrix} P_{\mathrm{ref}} \\ Q_{\mathrm{ref}} \end{bmatrix} - \begin{bmatrix} P_V \\ Q_V \end{bmatrix} + \frac{K_s T_s}{z-1} \begin{bmatrix} P - P_{\mathrm{ref}} \\ Q - Q_{\mathrm{ref}} \end{bmatrix} \tag{24}$$

where $R(z)$ is the z-transform of the reference signal $r[k]$, and P and Q represent the unfiltered measured power injected to the main grid.

D. Voltage Regulation and Proportional Power Sharing Using Droop Control Concept for Islanded Mode

In grid-connected mode, the aforementioned LQR-ORT controller regulates the power sharing to the main grid. In this mode, the grid sets the ac bus voltage to nominal values. In islanded mode, all inverters must regulate the ac bus voltage and frequency while delivering active and reactive power to the loads. Also, each inverter must inject power proportionally according to its own rated power capacity.

As the LQR-ORT controller is based on the regulation of the output current (6), it is necessary to add a supplementary loop in order to regulate the output voltage in islanded mode. The output of this voltage controller is the power reference for the LQR-ORT controller to drive the output voltage to reference values. Control scheme for the voltage control loop is shown in Fig. 3. When main grid connection lost is detected, the voltage in the ac bus drops and grid connection flag becomes zero, activating the voltage controller. The detection of grid disconnection is assumed, and its development is out of the scope of this article. According to (6), it can be inferred that V_{cd} is directly proportional to the active power and V_{cq} is negatively proportional to the reactive power.

Using a PI compensator, the expression for the voltage controller is given by

$$\begin{bmatrix} P_{\mathrm{ref}} \\ Q_{\mathrm{ref}} \end{bmatrix} = \left(\frac{K_{iv} T_s}{z-1} + K_{pv} \right) \begin{bmatrix} 1 \\ -1 \end{bmatrix} \cdot \begin{bmatrix} V_{\mathrm{ref}d} - V_{cd} \\ V_{\mathrm{ref}q} - V_{cq} \end{bmatrix}. \tag{25}$$

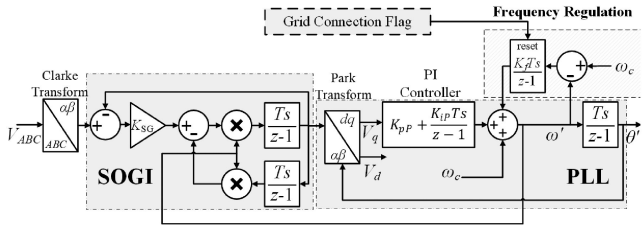

Fig. 4. SOGI-PLL with frequency regulation loop.

To distribute power sharing proportionally among the generators, a voltage-based droop control loop is implemented. The output of the droop control is subtracted from the output voltage reference as shown in Fig. 3. The expression for the voltage-based droop control is given by

$$\begin{bmatrix} V_{\mathrm{ref}d} \\ V_{\mathrm{ref}q} \end{bmatrix} = \begin{bmatrix} \bar{V}_d \\ 0 \end{bmatrix} - \begin{bmatrix} m \\ n \end{bmatrix} \cdot \begin{bmatrix} P \\ Q \end{bmatrix} \tag{26}$$

where $m \in \mathbb{R} > 0$ and $n \in \mathbb{R} < 0$ are known as the droop gains in d and q, respectively. To analyze power sharing, the following expression is obtained for two inverters:

$$\begin{bmatrix} V_{\mathrm{ref}d1} \\ V_{\mathrm{ref}q1} \end{bmatrix} + \begin{bmatrix} m_1 \\ n_1 \end{bmatrix} \cdot \begin{bmatrix} P_1 \\ Q_1 \end{bmatrix} = \begin{bmatrix} V_{\mathrm{ref}d2} \\ V_{\mathrm{ref}q2} \end{bmatrix} + \begin{bmatrix} m_2 \\ n_2 \end{bmatrix} \cdot \begin{bmatrix} P_2 \\ Q_2 \end{bmatrix}. \tag{27}$$

It is expected that in steady state, $V_{\mathrm{ref}d1} \cong V_{\mathrm{ref}d2}$ and $V_{\mathrm{ref}q1} \cong V_{\mathrm{ref}q2} \cong 0$. Then, the power sharing between j inverters will follow the rule

$$\begin{aligned} m_1 P_1 &\cong m_2 P_2 \ldots \cong m_j P_j \\ n_1 Q_1 &\cong n_2 P_2 \ldots \cong n_j Q_j. \end{aligned} \tag{28}$$

Notice that this droop control does not include frequency droop, since it occurs inherently in the frequency regulation loop presented in the following subsection.

E. Inverter Synchronization and Frequency Regulation

To synchronize each inverter with the ac bus, a second-order generalized integrator (SOGI-PLL) is implemented as shown in Fig. 4 [32]. The output of the SOGI-PLL is used to perform the *dq* transformation of the input and output signals of the LQR-ORT controller. When grid connection is lost, the operating frequency of the microgrid drops and the frequency regulation loop is activated. The frequency regulation loop integrates the frequency error and compensates the PLL operating frequency ω'. This way, the microgrid frequency operates around nominal values in islanded mode.

The expression of the output frequency of the SOGI-PLL with the proposed frequency regulation loop is given by

$$\omega' = V_{gq} \left(K_{pP} + \frac{K_{iP} T_s}{z-1} \right) + \omega_c + \frac{F_g K_f T_s}{z-1} (\omega_c - \omega') \tag{29}$$

where F_g is zero when grid connection is lost and one when the grid is engaged. Applying the final value theorem and defining the frequency deviation as $\Delta\omega\ = (\omega_c - \omega')$, the steady-state

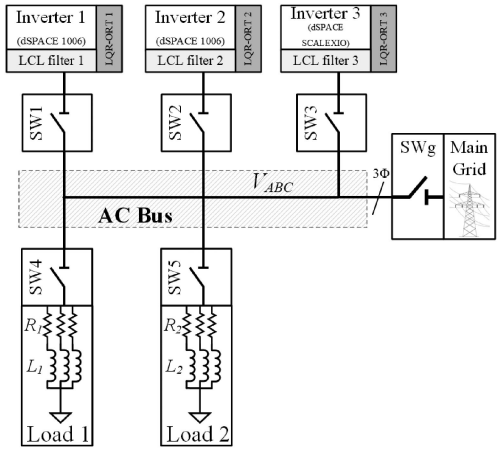

Fig. 5. Complete islanded microgrid scheme with *RL* load.

value of the frequency deviation is given by

$$\Delta\omega \;=\; -\frac{K_{iP}}{K_f}V_{gq}. \tag{30}$$

Equation (30) shows that the steady-state value of the frequency is directly related to the steady-state value of V_{gq}. This implies that the controlled microgrid has an inherent droop that modifies frequency according to load values.

IV. Study Case

To demonstrate the effectiveness of the LQR-ORT controller, a microgrid scenario with three inverter-based generators and two loads is proposed as shown in Fig. 5. There are connection switches located at the output of each inverter, at the input of each load, and at the point of connection with the main grid. Each inverter has its own LQR-ORT controller with the supplementary control loops. However, controllers for inverters 1 and 2 were implemented in a dSPACE 1006, and controller for inverter 3 was implemented in a dSPACE SCALEXIO. This is to validate the stability of the proposed frequency regulation loop under changes in clock frequency.

The parameter specifications used for this study case are summarized in Table I. To obtain the models of each inverter connected to the main grid, the component values were evaluated in (3) and (7) for each inverter. Also, to obtain the complete microgrid model in islanded mode, the component values were evaluated in (13) and (7). This resulted in three independent models for grid-connected mode and one model for islanded mode. The matrices Q_p and R_p were selected to obtain a settling time of 0.3 s under power references in grid-connected mode. The control feedback matrices K_{d1}, K_{d2}, and K_{d3} were computed using (16) and (17) and the selected weighing matrices. The matrix $K_\nu\nu_1$, $K_\nu\nu_2$, and $K_\nu\nu_3$ were obtained using (19) and (20) for each inverter. The outer integrator gain K_s was selected small to not have a significant effect on stability margins. The voltage droop gains were selected to provide an adequate power sharing among inverters according to their rated power. In addition, the voltage regulation gains were selected to reach steady state in less than 0.6 s for steps in loads. It is important to note that the selection of the voltage droop and voltage control gains do not have a predominant effect on the closed-loop stability due to the inherent robustness properties of the LQR-ORT controller.

TABLE I
Parameter Specification for the Study Case. Power Base: 1000 W. Voltage Base: 120 V_{RMS}

Parameter	Symbol	Value
Grid Voltage	V	1 p.u.
Grid Frequency	f	60 Hz
Output Inductance	L_{o1}, L_{o2}, L_{o3}	0.0471, 0.0471, 0.0942 p.u.
Input Inductance	L_{i1}, L_{i2}, L_{i3}	0.0471, 0.1413, 0.0942 p.u.
Filter Capacitance	C_1, C_2, C_3	0.7927×10^{-3} p.u.
PWM Frequency	f_{PWM}	$10kHz$
Sampling Period	T_s	$100\mu s$
Load 1, Load 2	$R_{1,2}, L_{1,2}$	5.95 p. u. (R), 10.73 p.u. (L)
LQR-ORT Controller		
Error Weighting Matrix	Q_{p1}, Q_{p2}, Q_{p3}	$\{5, 4.9, 4.8\}\times10^3\times I_{2\times2}$
Input Weighting Matrix	R_{p1}, R_{p2}, R_{p3}	$\{0.2, 0.15, 0.18\}\times I_{2\times2}$
Inner Integrator Gain	K_{i1}, K_{i2}, K_{i3}	1
Outer Integrator Gain	K_{s1}, K_{s2}, K_{s3}	5
SOGI gain	K_{SG}	0.7
PLL Gains (P, I)	K_{pP}, K_{iP}	0.28307, 7.5102
Voltage Control Gains (P, I)	K_{pv}, K_{iv}	10, 200
Frequency Regulation Gain	K_f	200
Power Rating	S_1, S_2, S_3	1.5, 1, 0.5 p.u.
Voltage Droop Gain (P-Vd)	m_1, m_2, m_3	0.04, 0.08, 0.12
Voltage Droop Gain (Q-Vq)	n_1, n_2, n_3	$-0.04, -0.08, -0.12$
Conventional Droop Controller		
Voltage Loop PR	K_{pV}, K_{rV}	0.35, 400
Current Loop PR	K_{pI}, K_{rI}	0.7, 100
Integral Frequency Droop	K_{iP1}	0.0015
Proportional Frequency Droop	m_{d1}, m_{d2}, m_{d3}	$\{3,6,9\}\times10^{-3}$
Proportional Amplitude Droop	n_{d1}, n_{d2}, n_{d3}	0.9, 0.18, 0.27

A. Robustness and Stability Analysis

To evaluate robustness and stability of the LQR-ORT controller, the islanded microgrid with load and frequency variations was analyzed. The load components were defined as randomized elements with a uniform variation in the range of $0 \rightarrow 7$ p.u. for *R* and $0 \rightarrow 50$ p.u. for *L*. Thus, 1000 instances of the microgrid model under load variations were created, and the stability was assessed using the nominal feedback control matrices K_{d1}, K_{d2}, and K_{d3}. Similarly, 1000 instances of the microgrid model under frequency variations were created.

To ensure that each inverter works independently without communications, the generalized feedback control matrix $K_{dT} = \mathrm{diag}(K_{d1}, K_{d2}, K_{d3})$ was defined. The controlled open loop microgrid $\Lambda_{\mu G} = K_{dT}\, G_{\mu G}$ is defined by

$$\Lambda_{\mu G}\;(z) = K_{dT}\left(zI - \bar{A}_{\mu G}\right)^{-1}\bar{B}_{\mu G} \tag{31}$$

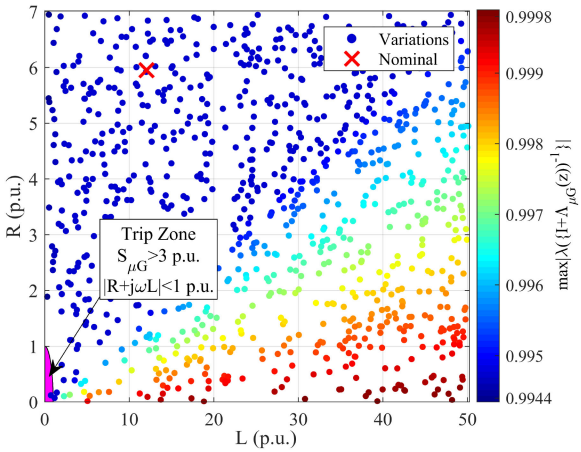

Fig. 6. Load variations and their effect on the closed-loop eigenvalues using the controller K_{dT} in islanded mode.

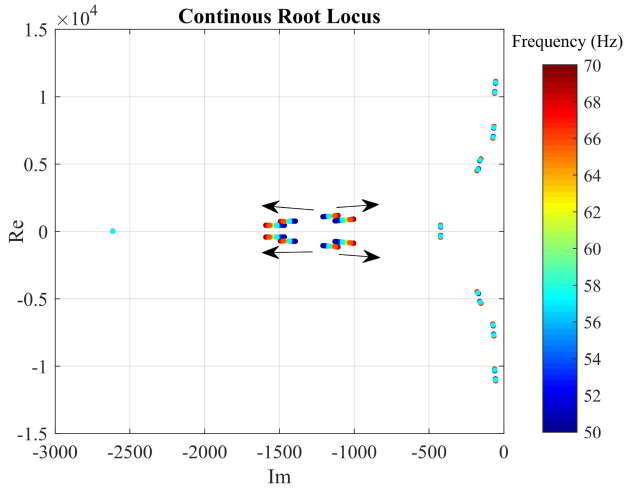

Fig. 7. Frequency variations and their effect on the closed-loop eigenvalues using the controller K_{dT} in islanded mode.

where $\bar{A}_{\mu G}$ and $\bar{B}_{\mu G}$ are the discrete time microgrid state and input matrices, respectively, from (13) transformed to the *dq* frame. The stability of the closed-loop microgrid was assessed by analyzing the return difference $I + \Lambda_{\mu G}(z)$, which defines the location of the closed-loop eigenvalues

$$\lambda\left\{(I+\Lambda_{\mu G}(z))^{-1}\right\} = \lambda\left\{\bar{A}_{\mu G} - \bar{B}_{\mu G} K_{dT}\right\}. \quad (32)$$

The operator $\lambda\{\cdot\}$ refers to the eigenvalue computation. The closed-loop microgrid becomes unstable if at least one of its eigenvalues has a magnitude greater than 1. Fig. 6 shows the load variations (R and L) and their effect on the maximum magnitude of the microgrid's discrete closed-loop eigenvalues.

The magnitude of the closed-loop eigenvalues tends to 1 as R becomes smaller and L becomes larger. None of the load variations generates a closed-loop eigenvalue greater than 1, even when using highly inductive loads such as industrial ac motors. The downward-left region describes load values that generate an impedance magnitude less than 1 p.u. In this region, the power demand becomes higher than the microgrid total capacity $S_{\mu G} = S_1 + S_2 + S_3 = 3$ p.u. This demand could cause inverters to trip and the microgrid to become unstable. None of the eigenvalues become unstable in the nearby of this region. This implies that the closed-loop microgrid is robust under variations in RL loads using the LQR-ORT controller. Also, Fig. 7 shows the effect of frequency variations in the location of the closed-loop eigenvalues in a continuous root locus. According to this, the frequency variations do not have major impact on the eigenvalue location, demonstrating the robustness of the LQR-ORT controller under frequency disturbances in the islanded microgrid.

The discrete LQR controller has robustness properties such as high gain margins and phase margins of at least 60′° [36]. Stability margins for the LQR-ORT controller were calculated using disk margin method [37]. The disk margin method is used for estimating structured robustness under multiplicative uncertainties for multiple-input multiple-output (MIMO) systems. Thus, the nominal islanded microgrid has a gain margin of 12.10 dB and a phase margin of 42.68°, which is appropriate for the complete microgrid. These results demonstrate robustness and stability under component and load variations in the islanded microgrid.

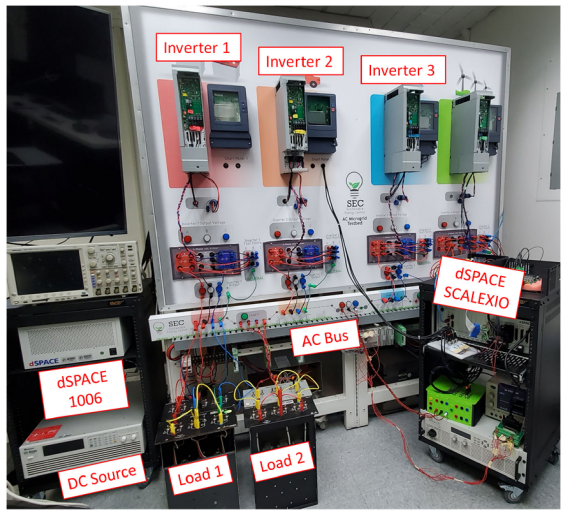

Fig. 8. Photograph of the experimental microgrid setup.

Finally, it is important to remark that the structure of the LQR-ORT controller makes the closed-loop generator robust under variations in the ac bus. This is because the power computation and the ac bus voltage are not included in the closed-loop state matrix $(\bar{A}_T - \bar{B}_T K_d)$ from (22). If V_{gdq} varies or if a disturbance is injected, the controller will not be optimal, and the performance will be slightly affected with an increase in settling time or overshoot.

B. Experimental Results

To evaluate the performance of the proposed control method, the microgrid test bed depicted in Fig. 8 has been used. This test bed consists of four Danfoss 2.2 kW inverters, voltage and current Life Energy Motion (LEM) sensors, *LCL* filters,

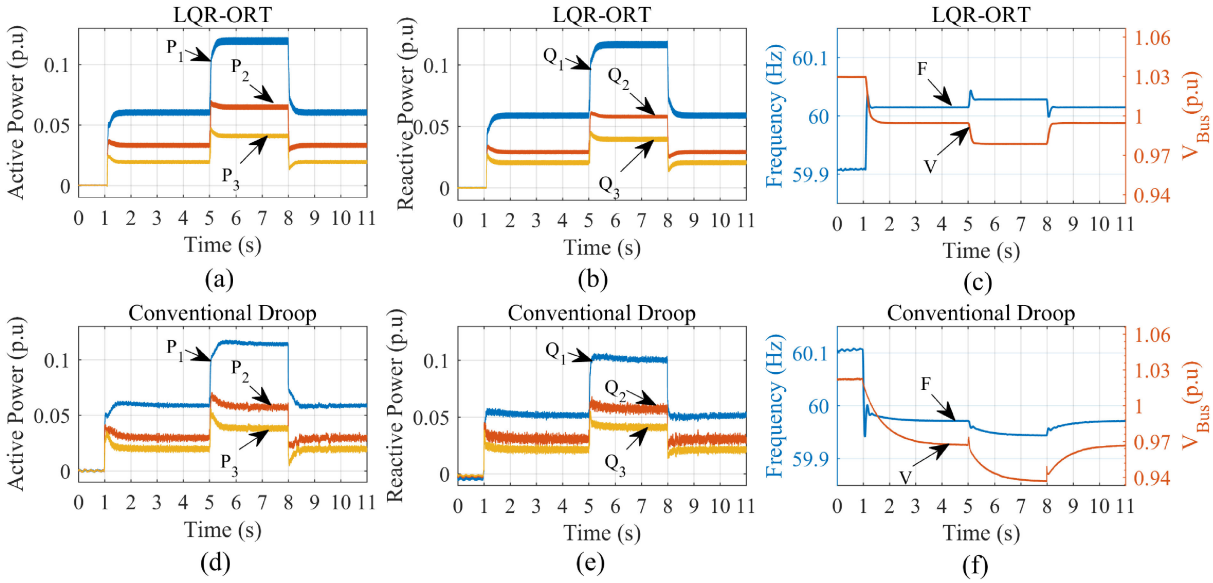

Fig. 9. Experimental results of the LQR-ORT compared to a conventional droop controller. (a) Active power LQR-ORT. (b) Reactive power LQR-ORT. (c) Voltage in the ac bus and frequency of the microgrid for the LQR-ORT. (d) Active power conventional droop controller. (e) Reactive power conventional droop controller. (f) Voltage in the ac bus and frequency of the microgrid for the conventional droop controller.

solid-state connection switches, a dSPACE1006, and a dSPACE SCALEXIO. The switching frequency of the inverters was set to 10 KHz using symmetric space-vector modulation. Refer to [38] for more details regarding the microgrid test bed.

The performance of the LQR-ORT controller was compared against a conventional droop controller from [1]. Control parameters of the conventional droop controller are also presented in Table I.

Fig. 9 shows the output power of each inverter, the rms voltage in the ac bus, and the microgrid frequency under different intervals of time for the LQR-ORT and the conventional droop controller. An LPF with a bandwidth of 100 rad/s was used in both controllers outside the control loop for power estimation.

At the beginning of the experiment (prior to $t = 1$ s), the ac bus is connected to the main grid. At this, each inverter works in grid following mode, which means that the main grid imposes the frequency and the voltage on the ac bus. Thus, the voltage in the ac bus and the frequency are deviated from their nominal values.

At $t = 1$ s, the main grid is disconnected and the microgrid starts working in islanded mode with load 1 connected. This means that inverters work together as grid forming generators to deliver the power demanded by load 1. At this time, the active power demanded by load 1 is correctly shared proportionally among inverters according to their rated power for both controllers [Fig. 9(a) and (d)]. However, the reactive power sharing for the LQR-ORT is improved compared to the conventional droop controller [Fig. 9(b) and (e)]. Regarding the transient response, the active and reactive powers reach steady state in 0.3 s for the LQR-ORT and 1.5 s for the conventional droop. Also, the active and reactive power waveforms of the LQR-ORT contain less noise compared to the conventional droop. AC bus voltage drops to 0.99 p.u. with a settling time of 1 s for the LQR-ORT, whereas the conventional droop controller voltage drops to 0.97 p.u. with a settling time of 4 s [Fig. 9(c) and (f)]. Also, microgrid frequency rises to 60.012 Hz with a settling time of 0.2 s for the LQR-ORT controller, whereas the conventional droop controller frequency drops to 59.97 Hz with a settling time of 3 s.

At $t = 5$ s, load 2 connection switch is closed. At this event, the settling time of the active and reactive power for the conventional droop increases to 2 s, whereas the LQR-ORT controller remains at 0.3 s. The voltage in the ac bus and frequency reach a value of 0.98 p.u. and 60.028 Hz, respectively, for the LQR-ORT, and 0.94 p.u. and 59.94 Hz for the conventional droop controller. Dynamics in the ac bus voltage and frequency of the LQR-ORT are faster than the conventional droop controller due to the lack of an LPF that separates the $V{-}I$ and power dynamics.

The waveforms of the output currents of each inverter for each controller are also shown in Fig. 9. It is shown that the transient response of the output currents is faster for the LQR-ORT compared to the conventional droop controller. Also, the output current waveforms of the LQR-ORT controller contain less noise compared to the conventional droop controller. This implies less power losses and better transient response.

Experimental results shown in Fig. 10 demonstrate that, compared to a conventional droop controller, the LQR-ORT improves the transient response of the islanded microgrid and also improves reactive power sharing among generators. The fast response of the ac bus voltage and frequency for the LQR-ORT controller occurs because this controller does not require LPFs inside the control loop. Also, the inherent robustness of the LQR-ORT controller allows the increase of voltage droop gains in order to improve transient response.

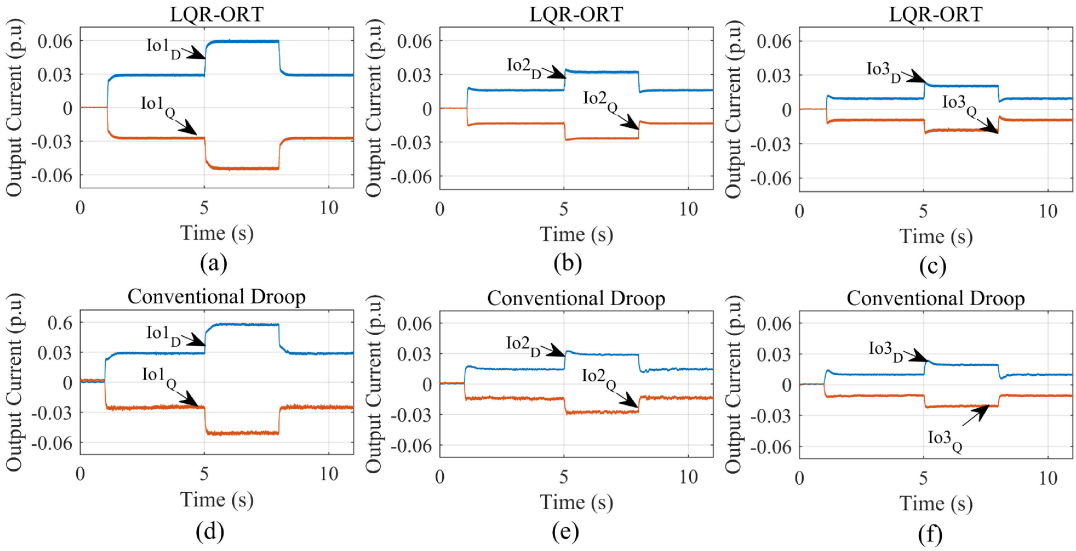

Fig. 10. Output currents in the *dq* frame during the experiment for the LQR-ORT controller and the conventional droop controller. (a) Inverter 1 LQR-ORT. (b) Inverter 2 LQR-ORT. (c) Inverter 3 LQR-ORT. (d) Inverter 1 conventional droop. (e) Inverter 2 conventional droop. (f) Inverter 3 conventional droop.

V. Conclusion

The proposed LQR-ORT controller for islanded and grid-connected microgrids improves transient response, accuracy on power sharing, and voltage and frequency regulation. It is worth mentioning that the frequency and voltage regulation is performed without communications, which improves reliability. The model presented in this article integrates $V{-}I$ and power sharing dynamics in a single state-space model. Using this new model allows to perform modern analysis methods for stability and robustness. Stability and robustness analysis show that the LQR-ORT controller has robust performance and stability under uncertainties in load. Experimental results have confirmed the benefits of the presented approach and its advantages compared to conventional droop controllers.

Appendix

Assuming the following state-space model for one phase oscillating at certain angular frequency ω

$$\dot{x} = Ax + Bu \tag{33}$$

with

$$A = \begin{bmatrix} a_{11} & \cdots & a_{1n} \\ \vdots & \ddots & \vdots \\ a_{n1} & \cdots & a_{nn} \end{bmatrix}, \; B = \begin{bmatrix} b_{11} & \cdots & b_{m1} \\ \vdots & \ddots & \vdots \\ b_{n1} & \cdots & b_{nm} \end{bmatrix},$$
$$x = \begin{bmatrix} x_1 \\ \vdots \\ x_n \end{bmatrix}, \; u = \begin{bmatrix} u_1 \\ \vdots \\ u_m \end{bmatrix}. \tag{34}$$

The following formula may be used to transform the balanced model from the *ABC* frame to the *dq* frame [39]:

$$A_{dq} = \begin{bmatrix} a_{T1} & a_{12}I_{2\times 2} & \cdots & a_{1n}I_{2\times 2} \\ a_{21}I_{2\times 2} & a_{T2} & \cdots & a_{2n}I_{2\times 2} \\ \vdots & \vdots & \ddots & \vdots \\ a_{n1}I_{2\times 2} & a_{n2}I_{2\times 2} & \cdots & a_{Tn} \end{bmatrix}, \; x_{dq} = \begin{bmatrix} x_{1d} \\ x_{1q} \\ \vdots \\ x_{nd} \\ x_{nq} \end{bmatrix}$$
$$B_{dq} = \begin{bmatrix} b_{11}I_{2\times 2} & \cdots & b_{1m}I_{2\times 2} \\ \vdots & \ddots & \vdots \\ b_{n1}I_{2\times 2} & \cdots & b_{nm}I_{2\times 2} \end{bmatrix}, \; u_{dq} = \begin{bmatrix} u_{1d} \\ u_{1q} \\ \vdots \\ u_{md} \\ u_{mq} \end{bmatrix} \tag{35}$$

where

$$a_{Tj} = a_{jj}\, I_{2\times 2} + \begin{bmatrix} 0 & \omega \\ -\omega & 0 \end{bmatrix} \tag{36}$$

with $1 \leq j \leq n$.

References

[1] J. C. Vasquez, J. M. Guerrero, M. Savaghebi, J. Eloy-Garcia, and R. Teodorescu, "Modeling, analysis, and design of stationary-reference-frame droop-controlled parallel three-phase voltage source inverters," *IEEE Trans. Ind. Electron.*, vol. 60, no. 4, pp. 1271–1280, Apr. 2013.

[2] Y. Han, P. Shen, X. Zhao, and J. M. Guerrero, "Control strategies for islanded microgrid using enhanced hierarchical control structure with multiple current-loop damping schemes," *IEEE Trans. Smart Grid*, vol. 8, no. 3, pp. 1139–1153, May 2017.

[3] Y. Han, H. Li, P. Shen, E. A. A. Coelho, and J. M. Guerrero, "Review of active and reactive power sharing strategies in hierarchical controlled microgrids," *IEEE Trans. Power Electron.*, vol. 32, no. 3, pp. 2427–2451, Mar. 2017.

[4] X. Guo, Z. Lu, B. Wang, X. Sun, L. Wang, and J. M. Guerrero, "Dynamic phasors-based modeling and stability analysis of droop-controlled inverters for microgrid applications," *IEEE Trans. Smart Grid*, vol. 5, no. 6, pp. 2980–2987, Nov. 2014.

[5] H. Han, X. Hou, J. Yang, J. Wu, M. Su, and J. M. Guerrero, "Review of power sharing control strategies for islanding operation of AC microgrids," *IEEE Trans. Smart Grid*, vol. 7, no. 1, pp. 200–215, Jan. 2016.
[6] Z. Li, C. Zang, P. Zeng, H. Yu, and S. Li, "Fully distributed hierarchical control of parallel grid-supporting inverters in islanded AC microgrids," *IEEE Trans. Ind. Informat.*, vol. 14, no. 2, pp. 679–690, Feb. 2018.
[7] W. Zhang, W. Wang, H. Liu, and D. Xu, "A disturbance rejection control strategy for droop-controlled inverter based on super-twisting algorithm," *IEEE Access*, vol. 7, pp. 27037–27046, 2019.
[8] Y. Guan, J. M. Guerrero, X. Zhao, J. C. Vasquez, and X. Guo, "A new way of controlling parallel-connected inverters by using synchronous-reference-frame virtual impedance loop—Part I: Control principle," *IEEE Trans. Power Electron.*, vol. 31, no. 6, pp. 4576–4593, Jun. 2016.
[9] J. M. Guerrero, L. Garcia de Vicuna, J. Matas, M. Castilla, and J. Miret, "A wireless controller to enhance dynamic performance of parallel inverters in distributed generation systems," *IEEE Trans. Power Electron.*, vol. 19, no. 5, pp. 1205–1213, Sep. 2004.
[10] J. M. Guerrero, J. C. Vasquez, J. Matas, L. G. De Vicuña, and M. Castilla, "Hierarchical control of droop-controlled AC and DC microgrids—A general approach toward standardization," *IEEE Trans. Ind. Electron.*, vol. 58, no. 1, pp. 158–172, Jan. 2011.
[11] E. A. A. Coelho, P. C. Cortizo, and P. F. D. Garcia, "Small-signal stability for parallel-connected inverters in stand-alone AC supply systems," *IEEE Trans. Ind. Appl.*, vol. 38, no. 2, pp. 533–542, Mar./Apr. 2002.
[12] E. A. A. Coelho, P. C. Cortizo, and P. F. D. Garcia, "Small signal stability for single phase inverter connected to stiff AC system," in *Proc. Conf. Rec. IEEE Ind. Appl. Conf. Thirty-Forth IAS Annu. Meet. (Cat. No.99CH36370)*, 1999, vol. 4, pp. 2180–2187.
[13] N. Pogaku, M. Prodanović, and T. C. Green, "Modeling, analysis, and testing of autonomous operation of an inverter-based microgrid," *IEEE Trans. Power Electron.*, vol. 22, no. 2, pp. 613–625, Mar. 2007.
[14] A. Bolzoni, G. M. Foglia, L. Frosio, M. F. Iacchetti, and R. Perini, "Impact of line and control parameters on droop stability in inverters for distributed generation," *IEEE Trans. Smart Grid*, vol. 9, no. 6, pp. 6656–6665, Nov. 2018.
[15] C. A. Macana and H. R. Pota, "Adaptive synchronous reference frame virtual impedance controller for accurate power sharing in islanded ac-microgrids: A faster alternative to the conventional droop control," in *Proc. IEEE Energy Convers. Congr. Expo.*, Oct. 2017, pp. 3728–3735.
[16] S. Tolani and P. Sensarma, "An instantaneous average current sharing scheme for parallel UPS modules," *IEEE Trans. Ind. Electron.*, vol. 64, no. 12, pp. 9210–9220, Dec. 2017.
[17] X. Meng, J. Liu, and Z. Liu, "A generalized droop control for grid-supporting inverter based on comparison between traditional droop control and virtual synchronous generator control," *IEEE Trans. Power Electron.*, vol. 34, no. 6, pp. 5416–5438, Jun. 2019.
[18] H. J. Avelar, W. A. Parreira, J. B. Vieira, L. C. G. De Freitas, and E. A. A. Coelho, "A state equation model of a single-phase grid-connected inverter using a droop control scheme with extra phase shift control action," *IEEE Trans. Ind. Electron.*, vol. 59, no. 3, pp. 1527–1537, Mar. 2012.
[19] R. Majumder, "Some aspects of stability in microgrids," *IEEE Trans. Power Syst.*, vol. 28, no. 3, pp. 3243–3252, Aug. 2013.
[20] Y. Deng, Y. Tao, G. Chen, G. Li, and X. He, "Enhanced power flow control for grid-connected droop-controlled inverters with improved stability," *IEEE Trans. Ind. Electron.*, vol. 64, no. 7, pp. 5919–5929, Jul. 2017.
[21] Q.-C. Zhong and Y. Zeng, "Universal droop control of inverters with different types of output impedance," *IEEE Access*, vol. 4, pp. 702–712, 2016.
[22] F. L. Lewis, D. L. Vrabie, and V. L. Syrmos, *Optimal Control*. Hoboken, NJ, USA: John Wiley & Sons, 2012.
[23] J. Maciejowski, *Multivariable Feedback Design*, vol. 1, no. 1. Harlow, U.K.: Addison Wesley, 1989.
[24] M. N. Marwali, J.-W. Jung, and A. Keyhani, "Control of distributed generation systems— Part II: Load sharing control," *IEEE Trans. Power Electron.*, vol. 19, no. 6, pp. 1551–1561, Nov. 2004.
[25] Y. A. R. I. Mohamed, H. H. Zeineldin, M. M. A. Salama, and R. Seethapathy, "Seamless formation and robust control of distributed generation microgrids via direct voltage control and optimized dynamic power sharing," *IEEE Trans. Power Electron.*, vol. 27, no. 3, pp. 1283–1294, Mar. 2012.
[26] R. Majumder, B. Chaudhuri, A. Ghosh, R. Majumder, G. Ledwich, and F. Zare, "Improvement of stability and load sharing in an autonomous microgrid using supplementary droop control loop," *IEEE Trans. Power Syst.*, vol. 25, no. 2, pp. 796–808, May 2010.
[27] H. Moussa, A. Shahin, J.-P. Martin, S. Pierfederici, and N. Moubayed, "Optimal angle droop for power sharing enhancement with stability improvement in islanded microgrids," *IEEE Trans. Smart Grid*, vol. 9, no. 5, pp. 5014–5026, Sep. 2018.
[28] M. Eskandari, L. Li, and M. H. Moradi, "Decentralized optimal servo control system for implementing instantaneous reactive power sharing in microgrids," *IEEE Trans. Sustain. Energy*, vol. 9, no. 2, pp. 525–537, Apr. 2018.
[29] J. M. Rey, P. P. Vergara, M. Castilla, A. Camacho, M. Velasco, and P. Martí, "Droop-free hierarchical control strategy for inverter-based AC microgrids," *IET Power Electron.*, vol. 13, no. 7, pp. 1403–1415, May 2020.
[30] J. F. Patarroyo-Montenegro, J. D. Vasquez-plaza, F. Andrade, G. Beauchamp, and L. Fan, "An optimal power control strategy for grid-following inverters in a synchronous frame," *Appl. Sci.*, vol. 10, no. 19, Sep. 2020, Art. no. 6730.
[31] J. F. Patarroyo-Montenegro, J. D. Vasquez-Plaza, and F. Andrade, "A state-space model of an inverter-based microgrid for multivariable feedback control analysis and design," *Energies*, vol. 13, no. 12, pp. 1–29, Jun. 2020.
[32] R. Teodorescu, M. Liserre, and P. Rodríguez, *Grid Converters for Photovoltaic and Wind Power Systems*. Chichester, U.K.: John Wiley & Sons, Ltd., 2011.
[33] *Standard for Interconnection and Interoperability of Distributed Energy Resources with Associated Electric Power Systems Interfaces*, IEEE Std. 1547-2018, IEEE Standard Association, 2018.
[34] M. Lu, X. Wang, P. C. Loh, F. Blaabjerg, and T. Dragicevic, "Graphical evaluation of time-delay compensation techniques for digitally controlled converters," *IEEE Trans. Power Electron.*, vol. 33, no. 3, pp. 2601–2614, Mar. 2018.
[35] N.-Z. Y. Fei-Hu and Y.-T. Juang, "Optimal controller of a buck DC-DC converter using the uncertain load as stochastic noise," *IEEE Trans. Circuits Syst. II Express Briefs*, vol. 52, no. 2, pp. 77–81, Feb. 2005.
[36] K. G. Arvanitis, G. Kalogeropoulos, and S. Giotopoulos, "Guaranteed stability margins and singular value properties of the discrete-time linear quadratic optimal regulator," *IMA J. Math. Control Inf.*, vol. 18, no. 3, pp. 299–324, 2001.
[37] J. D. Blight, R. L. Dailey, and D. Gangsaas, "Practical control law design for aircraft using multivariable techniques," *Int. J. Control*, vol. 59, no. 1, pp. 93–137, 1994.
[38] J. F. Patarroyo-Montenegro, J. E. Salazar-Duque, S. I. Alzate-Drada, J. D. Vasquez-Plaza, and F. Andrade, "An AC microgrid testbed for power electronics courses in the University of Puerto Rico at Mayagüez," 2018, doi: 10.1109/ANDESCON.2018.8564636.
[39] J. Pou, "Modulation and control of three-phase PWM converters," Ph.D. dissertation, Dept. Elect. Eng., Univ. Politècnica de Catalunya, Terrassa, Spain, 2002.

Juan F. Patarroyo-Montenegro (Member, IEEE) received the B.S. degree in electronics engineering from the University of Quindio, Armenia, Colombia, in 2011, the M.S. and Ph.D. degrees in automatic control from the University of Puerto Rico-Mayaguez (UPRM), Mayaguez, Puerto Rico, USA, in 2015 and 2019, respectively.

In 2017, he joined as the Laboratory Coordinator with the Sustainable Energy Center (SEC), UPRM, wherer he is currently working as a Postdoctoral Researcher. His main research interests include optimal and robust control systems, embedded systems and modeling, analysis, control, and design of power electronic converters, principally dc/ac power conversion.

Fabio Andrade (Member, IEEE) received the Ph.D. degree from the Universitat Politècnica de Catalunya (UPC), Barcelona, Spain, in 2013, and the B.Sc. degree in electronic engineering and the master's degree in engineering with emphasis on automatic control from the Universidad Del Valle, Cali, Colombia, in 2004 and 2007, respectively.

In 2009, he joined the Motion Control and Industrial Centre Innovation Electronics (MCIA). In 2014, he was a Postdoctoral Researcher with UPC and Aalborg University, Aalborg, Denmark. Currently, he is the Director of the Sustainable Energy Center (SEC) and an Associate Professor on power electronics applied to renewable energy with the University of Puerto Rico, Mayaguez Campus, Puerto Rico, USA. His main research interests include modeling, analysis, design, and control of power electronic converters, principally for dc/ac power conversion, grid-connection of renewable energy sources, and microgrid application.

Josep M. Guerrero (Fellow, IEEE) received the B.S. degree in telecommunications engineering, the M.S. degree in electronics engineering, and the Ph.D. degree in power electronics from the Technical University of Catalonia, Barcelona, Spain, in 1997, 2000, and 2003, respectively.

Since 2011, he has been a Full Professor with the Department of Energy Technology, Aalborg University, Aalborg, Denmark, where he is responsible for the Microgrid Research Program. From 2014, he has been a Chair Professor with Shandong University, Shandong, China. Since 2015, he has been a Distinguished Guest Professor with Hunan University, Changsha, China. Since 2016, he has been a Visiting Professor Fellow with Aston University, Birmingham, U.K., and a Guest Professor with the Nanjing University of Posts and Telecommunications, Nanjing, China. From 2019, he has been a Villum Investigator with the Villum Fonden, which supports the Center for Research on Microgrids (CROM) at Aalborg University, with him being the Founder and Director of the same center. His research interests include different microgrid aspects, including power electronics, distributed energy-storage systems, hierarchical and cooperative control, energy management systems, smart metering, and the Internet of Things for ac/dc microgrid clusters and islanded minigrids, especially focused on microgrid technologies applied to offshore wind, maritime microgrids for electrical ships, vessels, ferries, and seaports, and space microgrids applied to nanosatellites and spacecrafts.

Prof. Guerrero is an Associate Editor for a number of IEEE transactions. He has authored or coauthored more than 600 journal papers in the fields of microgrids and renewable energy systems, which have been cited more than 50 000 times. He was the recipient of the Best Paper Award of the IEEE TRANSACTIONS ON ENERGY CONVERSION for the 2014–2015 period, and the Best Paper Prize of *IEEE-PES*, in 2015. He was also was the recipient of the Best Paper Award of the *Journal of Power Electronics*, in 2016. From 2014 to 2020, he was awarded by Clarivate Analytics (formerly Thomson Reuters) as a Highly Cited Researcher with 50 highly cited papers.

Juan C. Vasquez (Senior Member, IEEE) received the B.S. degree in electronics engineering from the Autonomous University of Manizales, Manizales, Colombia, in 2004, and the Ph.D. degree in automatic control, robotics, and computer vision from Barcelona Tech-UPC, Barcelona, Spain, in 2009.

In 2011, he was an Assistant Professor, and in 2014, an Associate Professor with the Department of Energy Technology, Aalborg University, Aalborg, Denmark. In 2019, he became a Professor of energy Internet and microgrids, and is currently the Co-Director with the Villum Center for Research on Microgrids. He was a Visiting Scholar with the Center of Power Electronics Systems (CPES), Virginia Tech, Blacksburg, VA, USA, and a Visiting Professor with Ritsumeikan University, Kyoto, Japan. His current research interests include operation, advanced hierarchical, and cooperative control, optimization and energy management applied to distributed generation in ac/dc microgrids, maritime microgrids, advanced metering infrastructures, and the integration of Internet of Things and energy Internet into the SmartGrid.

Prof. Vasquez was an Associate Editor for *IET Power Electronics* and a Guest Editor for the IEEE TRANSACTIONS ON INDUSTRIAL INFORMATICS Special Issue on Energy Internet. He has been recognized as a Highly Cited Researcher by Thomson Reuters, since 2017, and was the recipient of the Young Investigator Award, in 2019. He has authored or coauthored more than 460 journal papers in the field of microgrids, which in total have been cited more than 19 500 times. He is currently a member of the IEC System Evaluation Group SEG4 on LVDC Distribution and Safety for Use in Developed and Developing Economies, the Renewable Energy Systems Technical Committee TC-RES in IEEE Industrial Electronics, PELS, IAS, and PES Societies.